ASIAN JOURNAL OF CIVIL ENGINEERING (BUILDING AND HOUSING) VOL. 10, NO. 5 (2009)
PAGES **-**

EFFECT OF LATERAL QUASI-STATIC LOAD ON NONLINEAR BEHAVIOUR AND DAMAGE INDEXES OF RETROFITTED RC FRAME MODEL

A. Vimuttasoongviriya*, N. Kwatra and M. Kumar
[a]Department of Civil Engineering, Thapar University, Patiala 147004, India

ABSTRACT

Existing reinforced concrete buildings in north India were built at times when seismic zones were not recognized. These buildings need to monitor the damage and improve their load carrying capacities for the purpose of seismic safety. This paper investigates the effect of lateral load on the damage index of reinforced concrete frame model strengthened using FRP sheets. Stiffness damage index and combined damage parameters approach were used. Change in modal parameters methods were investigated with the help of impact hammer excitation test. Finally, finite element method was used for modelling, nonlinear analysis and results processing of the specimen.

Keywords: Damage index, retrofitted RC frame model, FRP sheet, nonlinear FE method

1. INTRODUCTION

In north India, existing reinforced concrete (RC) buildings were constructed at time when seismic zones were not recognized. Therefore, they have inadequate reinforcement detailing which not results in deficient lateral load resistance. For the purpose of assuring seismic safety, it is necessary to detect the damaged state. Kanwar et.al [1] found that non-ductile RC moment resisting frames result in the need of retrofitting to increase the load resistance capacities. There are various methods of strengthening the damaged structures. The use of steel plate jacket and ferro-cement jacket are disruptive to the operation of the facility, labor intensive and time consuming. The Fiber Reinforcement Polymer (FRP) is one popular strengthening technique because FRP with epoxy have received considerable attention due to its high strength, light weight, quick and easy manageability on-site and high resistance against corrosion. This advance material has been successfully used to increase bending and shear capacity of flexural elements [2,3]. The retrofitted columns using FRP sheets have shown to prevent its brittle shear failure and also significantly improved their displacement ductility and energy dissipation capacity [4]. The use of FRP systems have also found to be an effective method for upgrading deficient RC connections [5].

*Email address of the corresponding author: atiwat.vimut@gmail.com (A. Vimuttasoongviriya)

For the purpose of structural damage assessment, it is necessary to monitor the structures for location and extent of damage. Damage index is a quantity that is used for estimating the damage status. This index depends on different specific damage parameters such as deformation, structural stiffness, energy dissipation and dynamic properties of structure. The well known combined damage index method is proposed by Park and Ang [6]. This index is calculated as a linear combination of maximum displacement response and total hysteretic energy dissipation under cyclic load. Powell and Allahabadi [7] introduced a deformation based damage index in terms of displacement or ductility. Kanvar et al. [8] suggested the method of stiffness damage assessment wherein the damage indicator is based on changes in the stiffness. Damage detection by calculating the change in modal parameters has been widely applied in damage alarming in health monitoring systems of highway bridges [9]. Dipasquale and Cakmak [10] presented damage index based on the change ratio of frequency. This method considers structural fundamental natural frequencies before and after damaged. Rodriguez and Barroso [11] and Wang et al. [12] proposed stiffness-mass ratios damage theory. This damage index is based on stiffness-mass ratio in form of modal parameters. The Modal flexibility damage index method is the well known one [13]. The principle of this method is on the basis of the comparison of the flexibility matrices obtained from two sets of mode shapes.

Response of whole building subjected to external load is a problem which is important to understand and there is little point in performing analysis without testing. This paper intends to investigate both damage indexes and effects on retrofitted RC frame model under quasi-static loads. Effect of FRP wraps on RC elements has been reported. The first part involves determination of load-deformation relationships. Change in stiffness, displacement ductility and energy dissipation have been investigated. Some of the damage indexes have been selected to indicate the damage for both nonlinear static and dynamic damage parameters approach. Subsequently, the ATENA-3D finite element program has been used for modelling, nonlinear analysis and results processing of the specimen. Three-dimensional finite element (FE) model is developed to replicate the experimental RC frame before and after FRP strengthening. Modeling methodology and nonlinear analysis approach in ATENA-3D are presented.

2. DAMAGE INDEX METHODS

In structural damage detection, a quantity of damage index (*DI*) is used to monitor the damage status of structure. This value is equal to zero when there is no damage and is equal to one when total collapse occurs. There are various parameters of physical responses to formulate damage index of structure. These damage parameters can be classified as deformation, change in stiffness, energy dissipation and changes in dynamical parameters [14]. A damage index can involve a combination of one or more damage variables in its calculation. For classification from difference viewpoints, the local damage index indicates the damage of structural elements or a part of structure and the global damage index considers the damage of the whole structure. Some of more significant damage indexes were studied and presented in this paper.

2.1 Damage index based on deformation, energy dissipation and change in stiffness

2.1.1 Park and Ang damage index

Park and Ang [6] have formulated a well known damage index to estimate the level of damage in structures. This damage index contains the damage cause by the maximum deformation and the damage due to dissipated energy subjected to cyclic loading. Both components of damage are linearly combined:

$$DI_{PA} = \frac{\delta_{\max}}{\delta_u} + \frac{\beta}{\delta_u P_y} \int dE_h \tag{1}$$

where $\delta_{\max}$ is the maximum experienced deformation, δ_u is the ultimate deformation under monotonic loading, P_y is yield strength of the structure which can be calculated using nonlinear finite element analysis, $\int dE_h$ is the hysteretic energy absorbed by the structural element during the response history and β is a model constant parameter. They have suggested the relationship between damage index and various damage states as presented in Table 1.

Table 1. Relation between damage index and various damage states [6].

Damage State	**Damage Index, *DI***	**State of Building**
No Damage	0.0	No Damage
Slight Damage	0.0-0.1	No Damage
Minor Damage	0.1-0.25	Minor Damage
Moderate Damage	0.25-0.4	Repairable
Severe Damage	0.4-1.0	Beyond Repair
Collapse	> 1.0	Loss of Building

2.1.2 Stiffness damage index method

Kanwar et al [8] proposed stiffness damage index method that uses an indicator based on the relationship between the material stiffness properties of the undamaged and the damaged member of the structure. According to this method severity of damage is expressed as the fractional change in stiffness of an element:

$$DI_k = \frac{k_j - k_j^*}{k_j} = 1 - \frac{1}{\nu_j} \tag{2}$$

where ν_j is stiffness ratio, k_j and k_j^* are the initial stiffness and damage stiffness of the *j*th member. The asterisk (*) denotes the damage state.

2.2 Damage index base on change in dynamic characteristics

The change in dynamic characteristics of structure such as resonance frequency and mode shape is widely used to calculate the damage of structure because damage always accompanies the reduction of stiffness as well as modal frequency. This approach calls modal parameters damage index method. This method has been widely applied in damage alarming of highway bridge [9]. Damage in different locations and components actually leads to different frequency changes in various modes. In this paper, the change in dynamic characteristics of structure was investigated with the help of impact hammer excitation test. The Fast Fourier Transforms (FFT) analyzer was used to analyze and recorded dynamical data of damaged structure. The damage index definitions of change in dynamic characteristics are presented as follows.

2.2.1 Dipasquale and Cakmak damage index

Dipasquale and Cakmak [14] defined the modal plastic softening index for the one-dimensional case, where the fundamental eigen frequency is considered. This damage index is given by

$$DI_{Dip} = 1 - \frac{\omega^{*2}}{\omega^2} \tag{3}$$

where ω and ω^* are the fundamental eigen frequency and damage frequency parameter, respectively. In this paper, natural frequencies of structure had been measured from experimental test in form of frequency response function (FRF) plot. This plot gave FRF magnitude corresponding to resonance frequency of each mode.

2.2.2 Stiffness-mass ratios method

Rodriguez and Barroso, [11] and Wang et al. [12] presented the story damage index is based on stiffness-mass ratios method in form of structural modal parameters. Considering multi-degree of freedom (MDOF) system, the mass at each floor is lumped together, given by m_l. Similarly, the lateral stiffness of the l^{th} story from 1 to *n* is given by k_l. The equation of motion of the structure under excitation force *P(t)* can be written as

$$\mathbf{M}\ddot{\mathbf{x}}(t) + \mathbf{C}\dot{\mathbf{x}}(t) + \mathbf{K}\mathbf{x}(t) = \mathbf{P}(t) \tag{4}$$

where **M, C** and **K** are the system mass, damping and stiffness matrices. **x**(*t*) is vector of the floor displacement relative to the vector of excitation force **P**(*t*). From the matrix eigenvalue problem, whose solution gives the natural frequencies and mode shape of a system, we have:

$$\left[\mathbf{K} - \lambda\mathbf{M}\right]\mathbf{\Phi} = 0 \tag{5}$$

where λ is the eigenvalue, and $\mathbf{\Phi}$ is the mode shape corresponding to λ. The associated

natural frequency, ω is given by the square root of λ.

Substituting the extracted eigenvalue, λ_j in form of ω_j^2 and the mode shape, $\mathbf{\Phi}_j$ of the j^{th} modal frequency into Eq. (4), the following system of linear equations can be obtained:

$$\begin{aligned}
\left(k_1+k_2-\omega_j^2 m_1\right)\phi_{1j}-k_2\phi_{2j} &= 0\\
-k_2\phi_{1j}+\left(k_2+k_3-\omega_j^2 m_2\right)\phi_{2j}-k_3\phi_{3j} &= 0\\
\vdots &= \vdots\\
-k_l\phi_{l-1,j}+\left(k_l+k_{l+1}-\omega_j^2 m_l\right)\phi_{lj}-k_{l+1}\phi_{l+1,j} &= 0\\
\vdots &= \vdots\\
-k_n\phi_{n-1,j}+\left(k_n-\omega_j^2 m_n\right)\phi_{nj} &= 0
\end{aligned} \tag{6}$$

Solving equation (6), a general expression of the l^{th} story stiffness can be obtain as

$$k_l=\omega_j^2\sum_{i=1}^{n}\frac{m_i\phi_{ij}}{\Delta\phi_{lj}} \quad \text{for} \quad j=1,2,\ldots,n \tag{7}$$

$$\Delta\phi_{lj}=\begin{cases}\phi_{lj}-\phi_{(l-1)j}, & \text{for } l=2,3,...,n\\ \phi_{lj} & \text{for } l=1\end{cases} \tag{8}$$

Defining the damage of a structure as the reduction percentage of story stiffness before and after damage, and assuming that the floor mass does not change due to the damage. This damage index of each story can be expressed as

$$DI_{SMR}=1-\frac{k_l^{*}/m_l}{k_l/m_l} \tag{9}$$

For the uniform floor mass distribution and substituting the story stiffness from Eq. (7) and Eq. (8) into Eq. (9), represented as damage index can be written as

$$DI_{SMR}=1-\frac{\omega_j^{*2}\sum_{i=1}^{n}\frac{\phi_{ij}^{*}}{\Delta\phi_{lj}^{*}}}{\omega_j^{2}\sum_{i=1}^{n}\frac{\phi_{ij}}{\Delta\phi_{lj}}} \tag{10}$$

The value of this damage index can be obtained based on one set of modal parameters.

2.2.3 Modal flexibility damage index method

Ko et. al, [13] and Pandey and Biswas, [15] suggested modal flexibility damage index method. They found that cracks in structure leads to an increase in structural flexibility. The principle of modal flexibility damage index method is based on the comparison of flexibility matrices obtained from two sets of experimental fundamental frequency and mode shape. The method is applicable if the mode shapes are mass normalized to unity which implies that the estimation of structural mass is required. The damage index for the l^{th} story using modal flexibility is defined as

$$DI_{MFDI} = 1 - \frac{F_l}{F_l^*} = 1 - \frac{\sum_{i=1}^{n} \phi_{li}^2 / \omega_i^2}{\sum_{i=1}^{n} \phi_{li}^{*2} / \omega_i^{*2}} \tag{11}$$

where F_l and F_l^* are the diagonal terms at coordinate l of the modal flexibility matrix of undamaged and damaged structure.

3. EXPERIMENTAL PROGRAM

3.1 Material System

The concrete used in the RC frame model was grade M20 (20 MPa). The longitudinal steel reinforcements were deformed bars and steel quantity was provided as per provisions of IS-456. The steel bars exhibited yield strength of 415 MPa and a Young's modulus of 200 GPa. The glass fiber reinforced polymer (GFRP) was used. It had a tensile strength of 3.4 GPa, elastic modulus of 63 GPa and density of 2.6 g/cm^3. The thickness of GFRP sheet used is 0.34 mm. Table 2 presents the details of the materials.

Table 2. The details of the materials.

Compressive strength of concrete		**20 MPa**	
	Diameter	Yield	Ultimate
Tensile strength of steel bars (MPa)	10 mm	475.68 MPa	586.60 MPa
	8 mm	516.65 MPa	628.91 MPa
Mechanical properties of FRP laminate			
Fibre	Thickness	Density	Tensile	*E*

GFRP	0.34 mm	2.6 g/cm^3	3.4 GPa	63 GPa

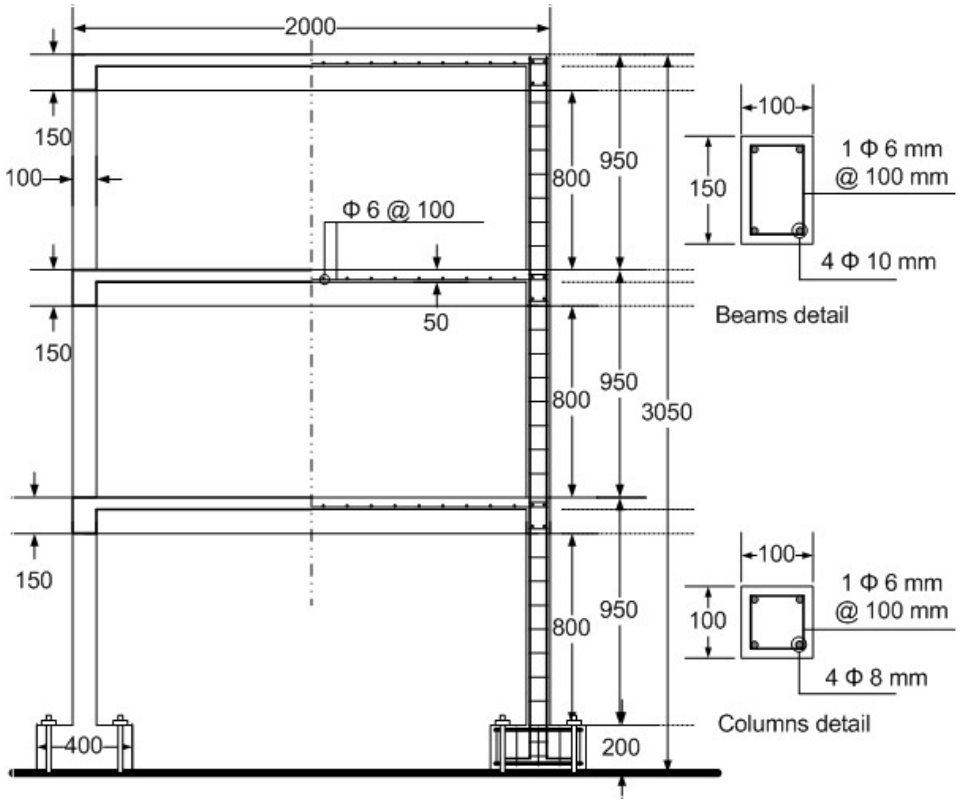

Figure 1. Schematic drawing of the model structure. All dimensions in millimeters

3.2 Specimen detail and testing procedure

A three story non-ductile RC moment resisting frame model was constructed in the laboratory. This frame built without beam-column joint transverse reinforcement bars. Each story was identical in most of the geometrical and mechanical aspects. The schematic drawing of the model is presented in Figure 1. The frame model consisted of three slabs 2000 mm x 2000 mm x 50 mm. Each column was equally sized with a rectangular cross section of 100 mm x 100 mm (reinforced with four 8 mm diameter bars) with a floor-to-floor height of 950 mm. All the beams were equally sized rectangular with a cross section of 100 mm x 150 mm (reinforced with two 10 mm diameter bars on the tension and compression faces). All columns and beams were provided with 6 mm diameter stirrups at 100mm centre-to-centre spacing. Each column was cast integrally with 150mm x 200mm x 400mm stub foundation. The stub was in turn bolted firmly on the strong floor. Each floor was equipped with one displacement dial gauge in the horizontal direction. A hydraulic jack of 200 kN capacity was horizontally installed along the desired direction at top floor. Quasi-static loads were applied at uniform pace rate to simulate structural damage. Applied load stories for both original and retrofitted frame are shown in Figure 2. Experimental test set-up

is shown in Figure 3.

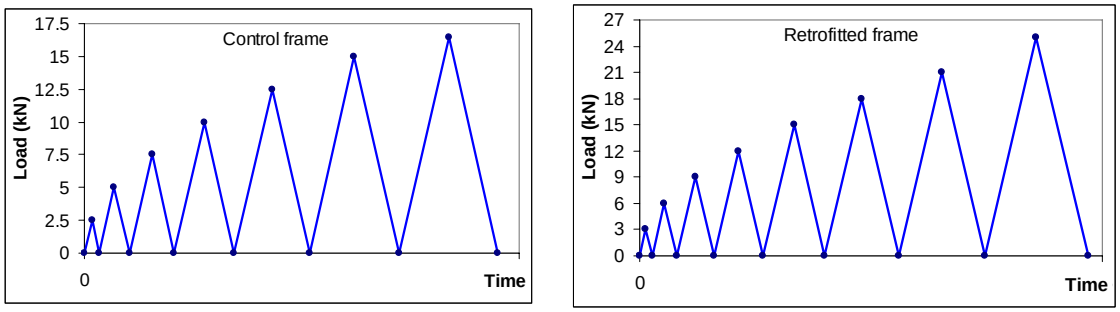

(a) (b)

Figure 2. Applied load history: a) control frame and b) retrofitted frame.

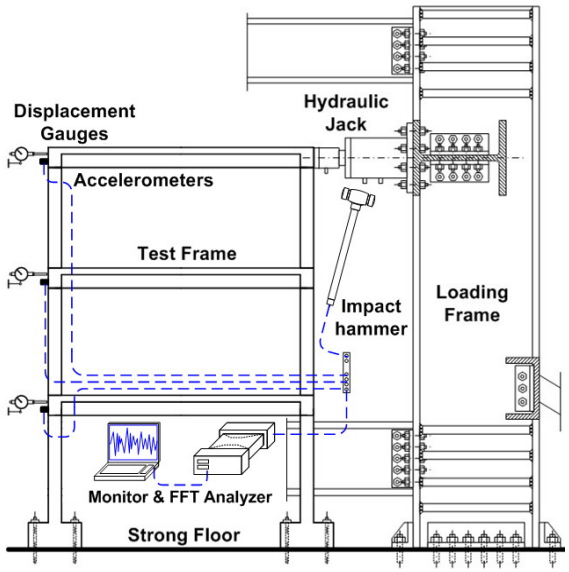

Figure 3. Experimental test set-up.

3.3 Impact hammer excitation test

Impact hammer excitation test is a useful tool because it gives information of the health of structure without destructing or affecting the facility when damage is hidden within the structure behind strengthening material layer. Each floor of experimental frame model was equipped with one accelerometer of 5kHz resonant frequency to measure vibration in horizontal direction. The accelerometer was mounted with a thin coating of epoxy on clean flat surface. Impact hammer of sensitivity 0.25mV/N with a hard rubber tip was used to excite the structure. Dynamic characteristic data of structure was automatically calculated and recorded by FFT spectrum analyzer. The usual aim of vibration measurement is to predict response given force in different damage status. The specific frequencies at which

resonance amplitudes occur are called the natural frequencies of the structure. These frequencies and the corresponding distribution of amplitude are global properties. Structural mode shapes are generalized from eigenvalue problem corresponding to natural frequencies.

3.4 Strengthening scheme

As earlier explained, the horizontal load was applied to the top floor of the control frame model till the desired damage state was reached. The damaged frame was then moved back to its initial state. Loose concrete was removed and the surfaces were cleaned of dirt. All the corners of damaged elements were beveled and rounded to a radius of 10 mm. The cracks were filled with epoxy layer of MBrace primer and surface was smoothed by MBrace concessive. Application of FRP wrap provided in two layers on to the damaged structure as shown in Figure 4. The first layer was provided with fiber oriented along the beam or column axes, to increase their flexural strength capacity. The columns and beams were confined at each edge zones by wrapping the other layer in the transverse direction as well. The schematic drawing of retrofitted frame is shown in Figure 5.

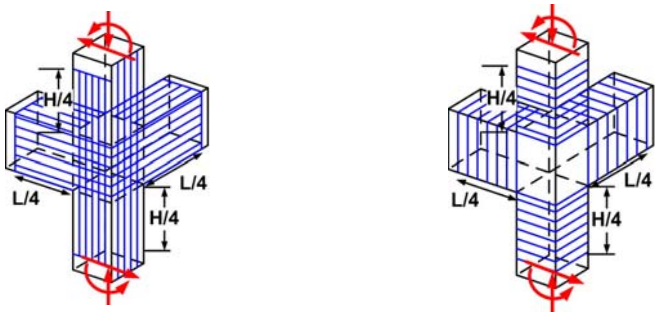

(a) (b)

Figure 4. Application of FRP wrap: a) flexural layers and b) confinement layers

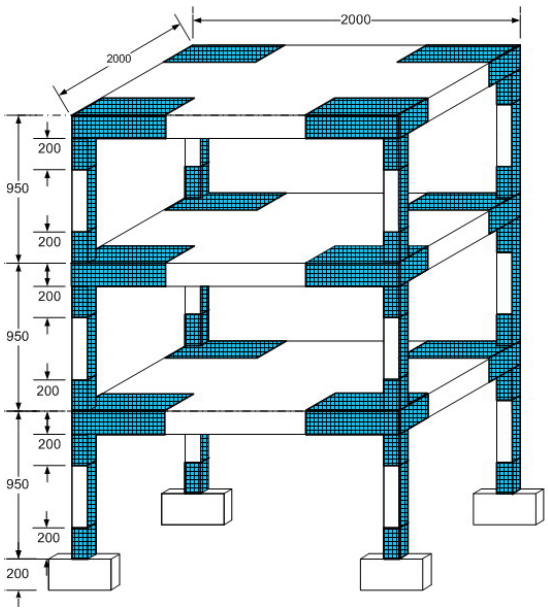

Figure 5. Schematic drawing of the retrofitted frame. All dimensions in millimeters

4. NONLINEAR FINITE ELEMENT ANALYSIS

In complicate analytical process of retrofitted RC structure with FRP sheets, simplified analysis tools cannot provide complete and accurate prediction. Finite element method is a numerical technique that it always uses to solve these difficulties. Many researchers are employed this technique to predict structural behavior and crack pattern of RC members [16]. Two-dimensional FE retrofitted beam models are studied by Supaviriyakit, et al. [17] and three-dimensional strengthened bridge models are investigated by Kachlakev, et al [18]. The ATENA nonlinear finite element program (ATENA-3D v4) was used in this study to simulate the behaviour of the RC frame. An eight-node brick element was used to model the concrete as shown in Figure 6. The element is capable of plastic deformation, cracking in three orthogonal directions and crushing. A polyline element was used to model the steel bars. Two nodes are required for this element. Each node has three degrees of freedom. The steel for the FE models was assumed to be an elastic-perfectly plastic material, Poisson's ratio of 0.3.

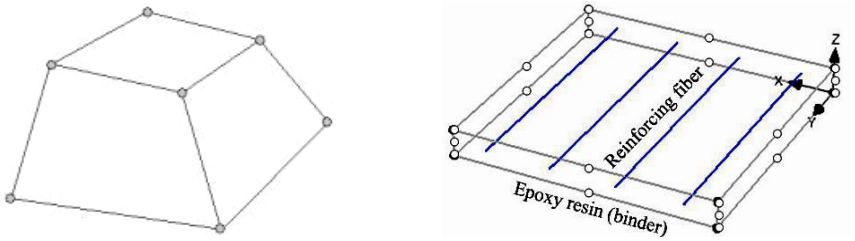

(a) (b)

Figure 6. a) An eight node brick element model and b) a schematic of FRP composite model

A shell element with 20 nodes, quadratic 3D brick element, was used to model the FRP composite. This element allows for different material layers with different orientations. FRP composite is that consist of two constituents. The constituents are combined at a macroscopic level and are not soluble in each other. One constituent is the reinforcement, which is embedded in the second constituent, epoxy, [18]. The reinforcing material is in the form of anisotropic materials of glass fibers, which are typically stiffer and stronger than the epoxy. Nodes of FRP layered shell elements were connected to those of adjacent concrete solid element in order to satisfy the perfect bond assumption. Figure 6 also shows a schematic of FRP composites. An eight-node brick element was used to model steel plates at the supports.

4.1 Material properties in ATENA nonlinear FE analysis

4.1.1 Equivalent uniaxial law

The nonlinear behavior of concrete in the biaxial stress state is described by the relationship

between effective stress σ_c^{ef} and the equivalent uniaxial strain ε^{eq}. The equivalent uniaxial strain is produced by the stress of concrete σ_{ci} with modulus E_{ci} associated with the direction *i*. The equivalent uniaxial strain is calculated as

$$\varepsilon^{eq} = \frac{\sigma_{ci}}{E_{ci}} \tag{12}$$

Unloading is a linear function to the origin. The equivalent uniaxial stress-strain diagram for concrete and an example of the unloading point *U* are shown in Figure 7. The relation between effective stress and equivalent uniaxial strain is not unique and depends on a load history.

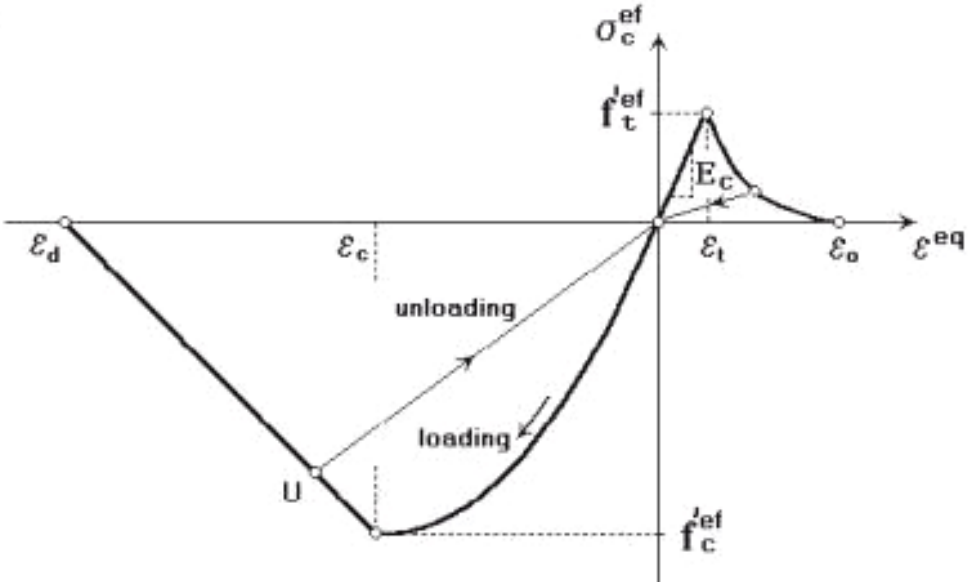

Figure 7. Uniaxial stress-strain relationship for concrete

4.1.2 Tension before cracking

The behavior of concrete in tension without cracks is assumed linear elastic from initial state to the effective tensile strength point. The tensile strength without cracks is calculated as

$$\sigma_c^{ef} = E_o \, \varepsilon^{eq} \qquad when \quad 0 \le \sigma_c \le f_t^{'ef} \tag{13}$$

where E_o is the initial elastic modulus of concrete, $f_t^{'ef}$ is the effective tensile strength derived from the biaxial failure function.

4.1.3 Tension after cracking

Exponential crack opening law was used to model the concrete crack opening in this paper.

The function of crack opening is calculated as

$$\frac{\sigma}{f_t^{'ef}} = \left\{1+\left(c_1\frac{w}{w_c}\right)^3\right\}\exp\left(-c_2\frac{w}{w_c}\right)-\frac{w}{w_c}\left(1+c_1^3\right)\exp\left(-c_2\right) \tag{14}$$

where w is the crack width, w_c is the crack opening at the complete release of stress, σ is the normal stress in the crack. Values of the constants are, c_1 = 3, c_2 = 6.93, respectively.

4.1.4 Compression before peak stress

The nonlinear behaviour of compression is following Committee Euro International du Beton model. The formula has been adopted for the ascending branch of the concrete stress-strain law in compression. This formula enables wide range of curve forms, and is appropriate for normal as well as high strength concrete.

$$\sigma_c^{ef} = f_c^{'ef}\frac{qx-x^2}{1+(q-2)x} \tag{15}$$

$$x=\frac{\varepsilon}{\varepsilon_c} \qquad and \qquad q=\frac{E_o}{E_c} \tag{16}$$

where $f_c^{'ef}$ is concrete effective compressive strength, x is normalized strain, q is shape parameter, ε is strain, ε_c is strain at the peak stress, E_o is initial elastic modulus and E_c is secant elastic modulus at the peak stress.

4.1.5 Compression after peak stress

This paper was used fictitious compression plane model to simulate compression after peak stress of concrete. The slope of the softening part of the stress-strain diagram is defined by two points: a peak of the diagram at the maximal stress and a limit compressive strain ε_d at the zero stress. This strain is calculated from a plastic displacement w_d and a band size L_d according to the following expression:

$$\varepsilon_d = \varepsilon_c + \frac{w_d}{L_d} \tag{17}$$

4.1.6 Compressive strength of cracked concrete

A reduction of the compressive strength after cracking in the direction parallel to the cracks in ATENA is calculated as following:

$$f_c^{'ef} = r_c \; f_c' \tag{18}$$

$$r_c = c + (1-c)e^{-(128\varepsilon_u)} \tag{19}$$

where r_c is compressive reduction factor, f_c' is compressive strength of concrete and constant c is 0.45, respectively.

4.1.7 Shear Stress in Cracked Concrete

The shear modulus is reduced with growing strain normal to the crack as shown in Figure 8 and this presents a reduction of the shear stiffness due to the crack opening.

$$G = r_g \; G_c \tag{20}$$

$$G_c = \frac{E_c}{2(1+\nu)} \tag{21}$$

where r_g is the shear retention factor, G is the reduced shear modulus, G_c is the initial concrete shear modulus, E_c is the initial elastic modulus and ν is the Poisson's ratio.

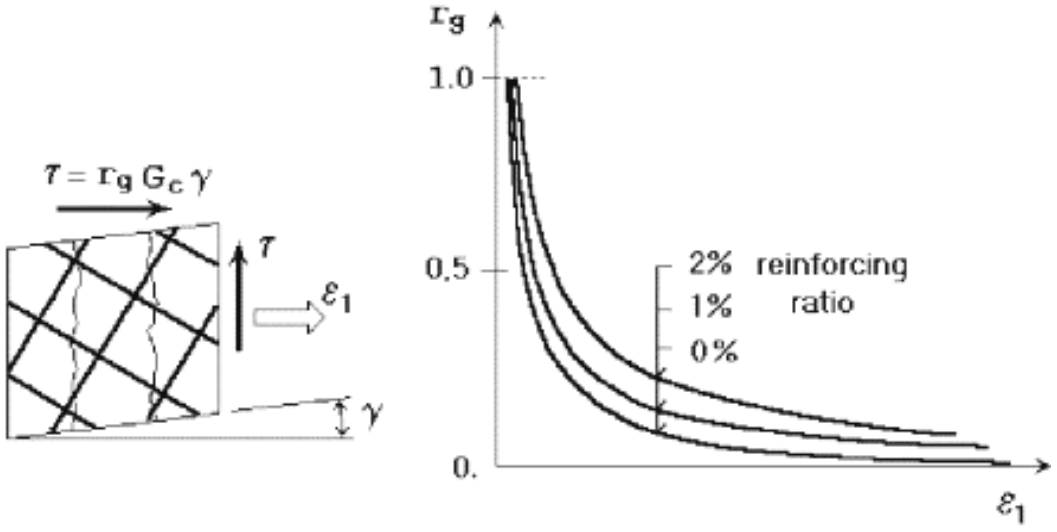

Figure 8. Shear retention factor

4.2 Loading, boundary conditions and nonlinear solution

By taking advantage of the symmetry of the frame, a symmetrical half of the full frame was used for modeling. The typical FE model for half of retrofitted frame is shown in Figure 9.

A one inch thick steel plate was added at the supporting and loading location in order to avoid stress concentration problems. At a plane of symmetry, the displacement in the direction perpendicular to the plane was held at zero. In nonlinear analysis, the loads applied to a finite element model are divided into a series of load increments called load steps. The ATENA program uses Newton-Raphson equilibrium iterations for updating the model stiffness. The monitoring points were measured at the middle of each floor, where the largest horizontal displacements can be expected.

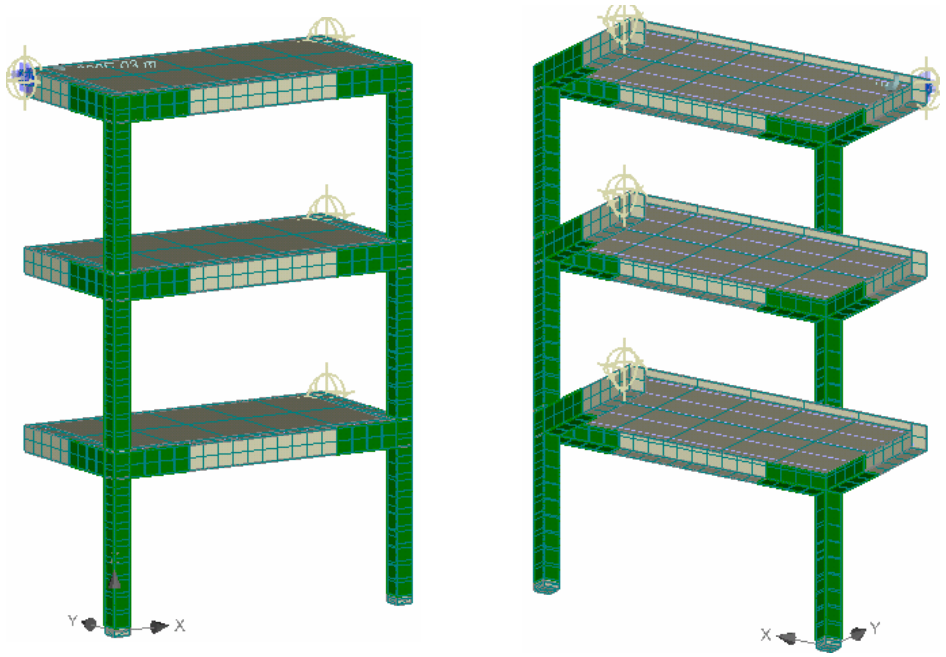

(a) (b)

Figure 9. FE model of retrofitted frame using FRP: a) outside view and b) inside view

5. RESULTS AND DISCUSSION

5.1 Load-displacement behaviour and correlation of damage indexes

5.1.1 Control frame

The control frame model was constructed and tested under lateral quasi-static load. Loads were applied at the middle of top floor. The changes of displacements with the increase of the number of quasi-static loads are given in Figure 10. The initial diagonal cracks occurred on the beam-column joints of the top floor at a load of 10kN, indicating that structural elements of top floor were the most stressed. The system damage index based on Park and Ang theory, DI_{Park} and stiffness damage index method, DI_k were 0.32 and 0.47, moderate damage state. At a load of 12.5 kN, large cracks started to open and small cracks occurred on connection joins of second floor. It indicated that the yield point was visible at a load

12.5kN, displacement of 31 mm from initial state, DI_{Park} of 0.49, DI_k of 0.57, severe damage state. Ultimate damage state began at the load of 16.5 kN and with a displacement of 69 mm, leading to DI_{Park} of 0.95 and DI_k of 0.76, respectively. The ductility index was nearly 2.22 and total energy dissipation was 567.57 kN-mm.

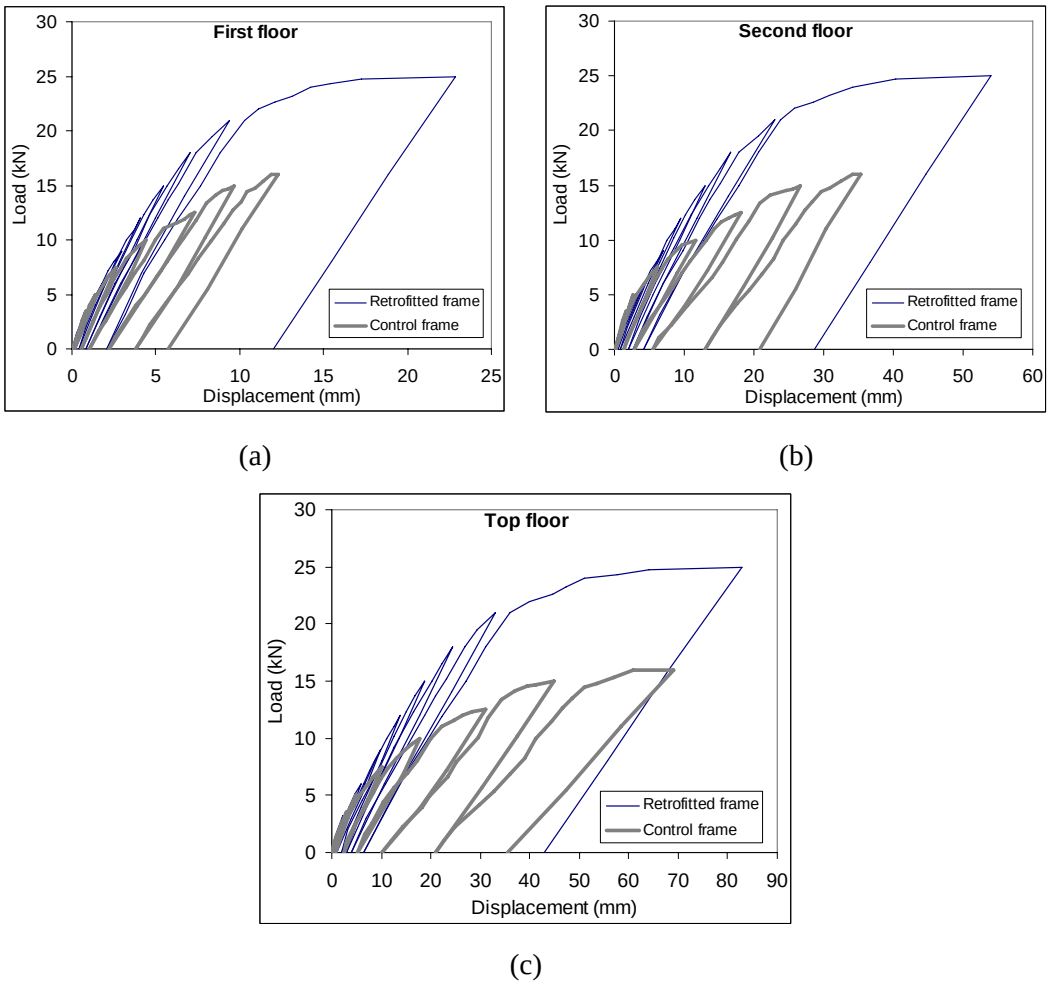

Figure 10. Load-displacement plots: a) first floor, b) second floor and c) top floor.

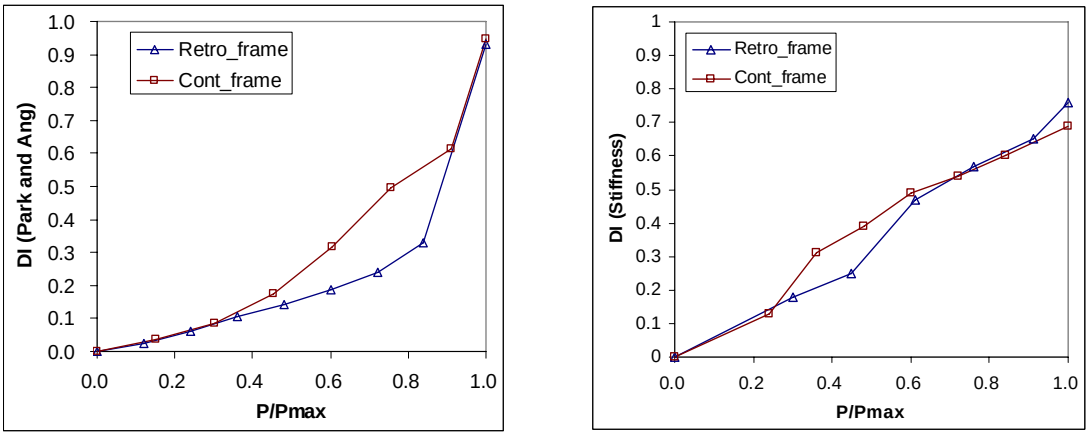

(a) (b)

Figure 11. a) *DI* of Park and Ang plots and b) *DI* of change in stiffness plots

Figure 11 presents the correlation between applied load ratio and DI_{Park} and DI_k, respectively. It shows that the value of DI_{Park} of control frame has two difference trends, while DI_k seem to increase in linear. The general trend of DI_{Park} is slightly changed because of the cumulative effects of low deformation and energy dissipation. The high deformation trend occurs after yield point. Based on high deformation trend, DI_{Park} changes shape when structure starts to lose their load carrying capacity. The value of DI_k seem to increase in linear manner because the initial stiffness ratio between undamaged and damaged structure change slowly as compare to other damage parameters such as displacement ratio and energy ratio. The summary of damage indexes and appearances of control frame are presented in Table 3.

Table 3. Damage index of structural system and appearance of control frame.

P,kN	P/P_{max}	DI_k	DI_{Park}	DI_{Dip}	DI_{SMR}	DI_{MFDI}	Appearance
0	0	0	0	0	0	0	Un-deformed
5.0	0.30	0.18	0.09	0.03	0.04	0.04	Un-cracked
7.5	0.45	0.25	0.18	0.06	0.09	0.09	Minor cracking
10.0	0.61	0.47	0.32	0.12	0.16	0.16	Moderate cracking
12.5	0.76	0.57	0.49	0.16	0.21	0.21	Severe cracking
15.0	0.91	0.65	0.61	0.25	0.27	0.26	Spalling of concrete cover
16.5	1	0.76	0.95	0.34	0.36	0.34	Loss of shear capacity

5.1.2 Retrofitted frame

Test for the retrofitted frame was performed in the similar manner as that for the control frame. At the final stage of the damaged control frame was grouting cracks by adhesive epoxy and wrapped it with FRP sheets. The load versus displacement behaviour and the change in damage indexes of retrofitted frame is shown in Figure 10 and 11 along with the behaviour of the control frame. The yield state of the retrofitted frame was visible at a load 18kN, displacement of 24.8mm. The system damage index of DI_{Park} and DI_k were 0.24 and 0.54, indicating that the frame was on severe damage state. The moving sound of FRP sheets started from the load of 18kN. The load displacement relation can be roughly considered to be linear when the load is smaller than or equal to yield point. Ultimate damage state was at the load of 25kN, displacement of 83 mm from initial state, total energy dissipation was 1039.68 kN-mm, DI_{Park} was 0.93 and DI_k was 0.69, respectively. There were breaking sounds of fiber and epoxy layers from connection joints at ultimate state. After remove FRP layers, it was observed that in addition to old cracks which opened up, new flexural cracks also appeared at the connection joints and columns.

Results from experiment test shows that the use of FRP wrapped for structural strengthening provides significant lateral load capacity increases approximately 151.5% as compared to control frame. The FRP wrapped around the structural elements in this manner are intended to provide external confinement and crushing of the concrete cover at larger lateral displacements. According to the change of structural displacements, the ductile behaviour of the retrofitted frame is largely restored after the FRP composite sheets are engaged. The summary of damage indexes and appearances of retrofitted frame are presented in Table 4. The health of non-ductile RC moment resisting structures of both original and strengthened specimen seemed to become unsafe when DI_{Park} and DI_k increases larger than 0.5 or structural stiffness reduces to more than 50% of initial state. DI_{Park} and DI_k of strengthened frame reduce indicating better performance as compare to the control frame.

Table 4. Damage index of structural system and appearance of retrofitted frame.

P,kN	P/P_{max}	DI_k	DI_{Park}	DI_{Dip}	DI_{SMR}	DI_{MFDI}	Appearance
0	0	0	0	0	0	0	Un-deformed
3.0	0.12	0.13	0.02	0.04	0.04	0.04	Un-cracked
9.0	0.36	0.39	0.10	0.08	0.10	0.10	Un-cracked
15.0	0.60	0.49	0.19	0.12	0.17	0.18	Noise of fibre moving
18.0	0.72	0.54	0.24	0.14	0.22	0.23	Severe damage
21.0	0.84	0.60	0.33	0.17	0.28	0.29	Breaking noise of fibre
25.0	1	0.69	0.93	0.30	0.34	0.35	Loss of shear capacity

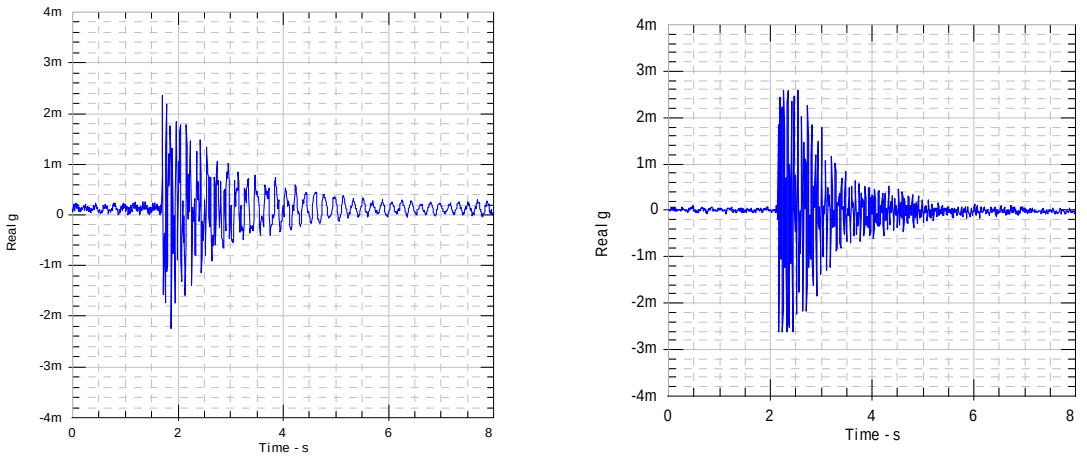

(a) (b)

Figure 12. Time history plot of control frame at top floor: a) initial state and b) final state

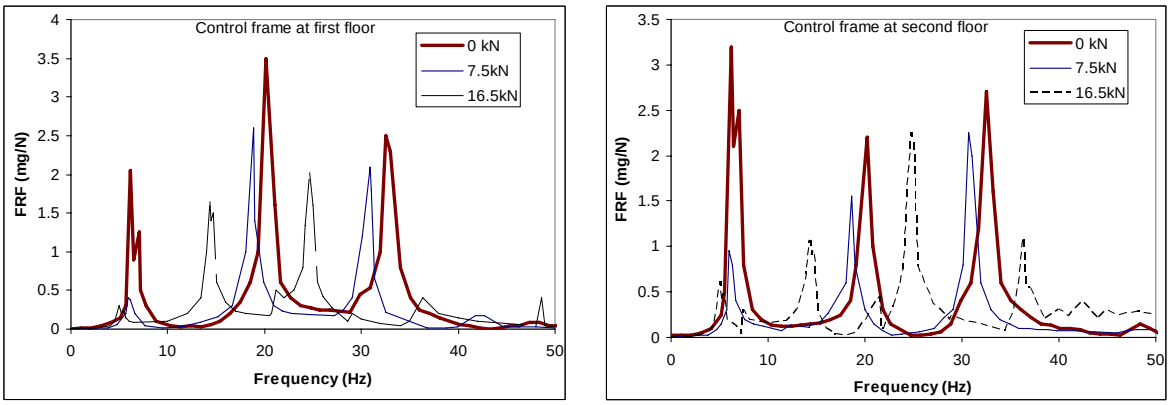

(a) (b)

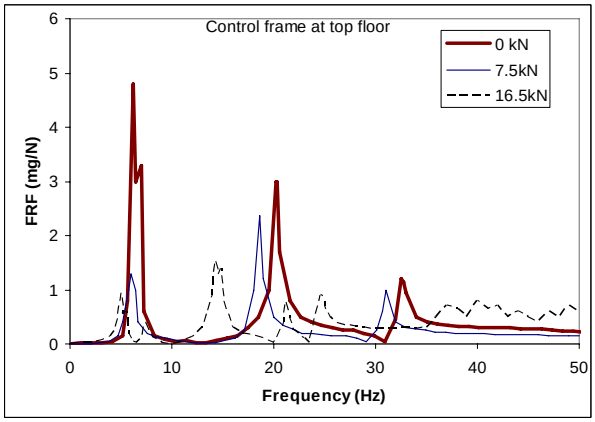

(c)

Figure 13. FRF plots of control frame a) first floor, b) second floor and c) top floor.

5.2 Dynamical characteristic results and damage indexes based on modal parameters

5.2.1 Control frame

After applied each load steps, the impact hammer was used to excite the testing frame model. The dynamic characteristics gave the records in FFT analyzer based on linear analysis setup. These records include trigger hammer plot, time history plot and frequency response function plot which give the amplitude of vibration along with frequency. The analyzer was set up to make a free zoom measurement with a frequency range of 0 to 50 Hz. In this frequency range there covered all three majority modes of this frame model. The time history plots are shown in Figure 12 and comparison of FRF plots of control frame are shown in Figure 13. At undamaged state the natural frequency at first, second and third mode were 6.5Hz, 19Hz and 31.5Hz. At initial cracks of 10 kN, DI_{Dip} was 0.12, DI_{SMR} was 0.16 and DI_{MFDI} was 0.16. At yield point of 12.5kN, the natural frequency at first, second and third mode were 5.5Hz, 17Hz and 27.2Hz. DI_{Dip} was 0.16, DI_{SMR} and DI_{MFDI} were 0.21, severe damage state. At ultimate damage state, DI_{Dip} was 0.34, DI_{SMR} was 0.36 and DI_{MFDI} was 0.34, respectively. The frequencies at ultimate state of first, second and third mode were 5.2 Hz, 15.5Hz and 25.9 Hz. The average changed of corresponding resonance frequency decreased approximately 18.73%.

The relation between applied loads and damage indexes based on modal parameters of control frame are shown in Figure 16 and 17. In order to estimate the dynamic properties of the frame under the damaged state, the measurements data after applied load are extracted to represent the behaviour of structure. It can be seen that DI_{Dip}, DI_{SMR} and DI_{MFDI} are small which agree with the fact that no visible damage was reported at load less than yield point. Meanwhile, some index values around 0.2 are obtained. In case of control frame, it is shown that the value of damage indexes based on change in frequency and mode shape both DI_{SMR} and DI_{MFDI} are slightly larger than the modal plastic softening index, DI_{Dip}. In order to estimate the modal parameter based index which compares only the natural frequency of structure with damage or undamaged structure, DI_{Dip} is more sensitive in the case of severe damage state or after large cracking. The results of damage indexes obtained show that the damage of structures for both control and retrofitted frame are said to be of great concern, when modal parameter damage indexes increase to larger than 0.20 or the structure experienced severe damage after yield load.

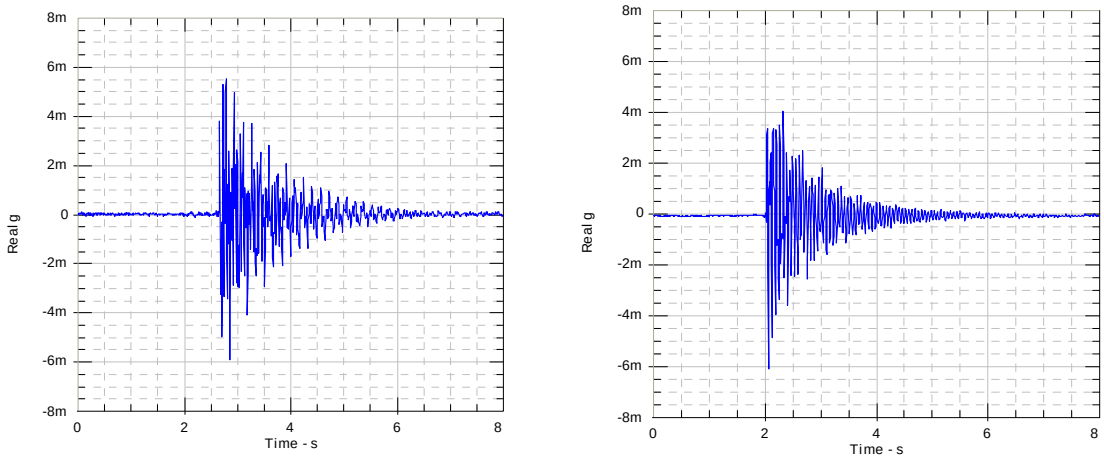

(a) (b)

Figure 14. Time history plot of retrofitted frame at top floor: a) initial state and b) final state

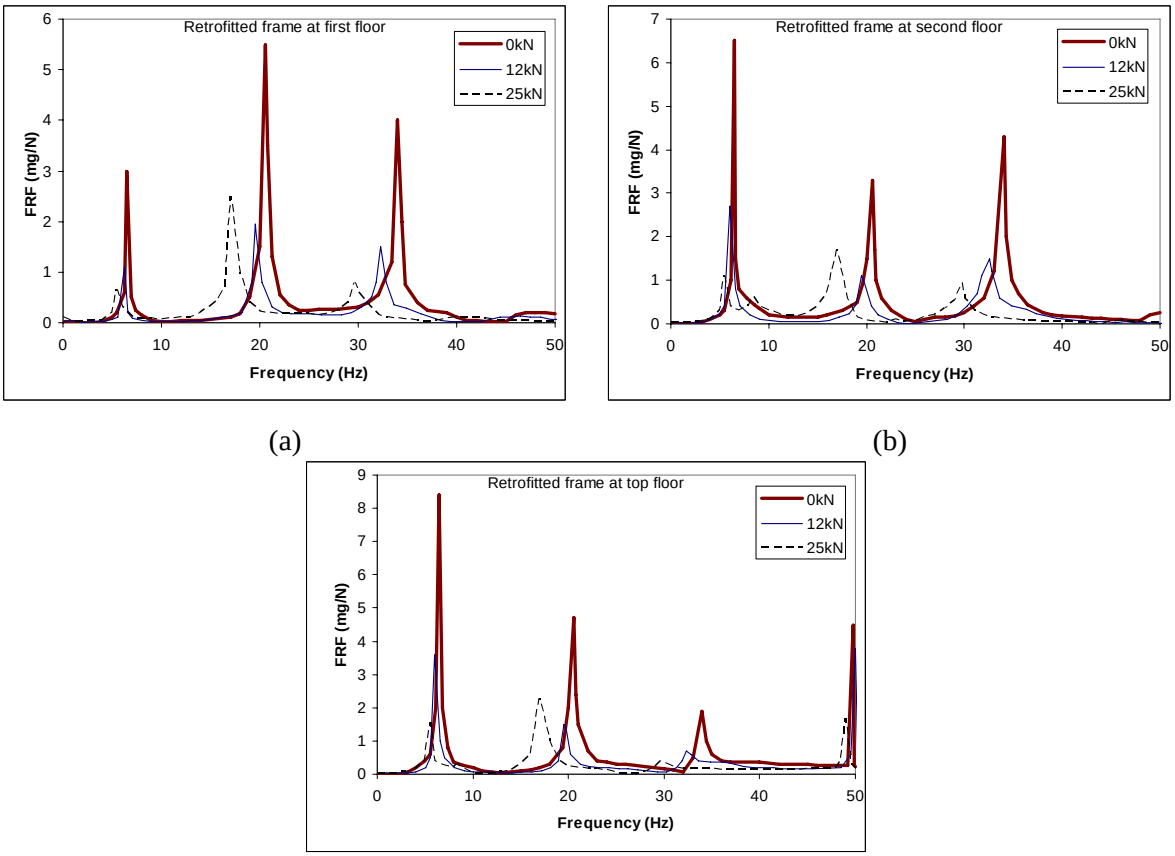

(a) (b)

(c)

Figure 15. FRF plots of retrofitted frame: a) first floor, b) second floor and c) top floor

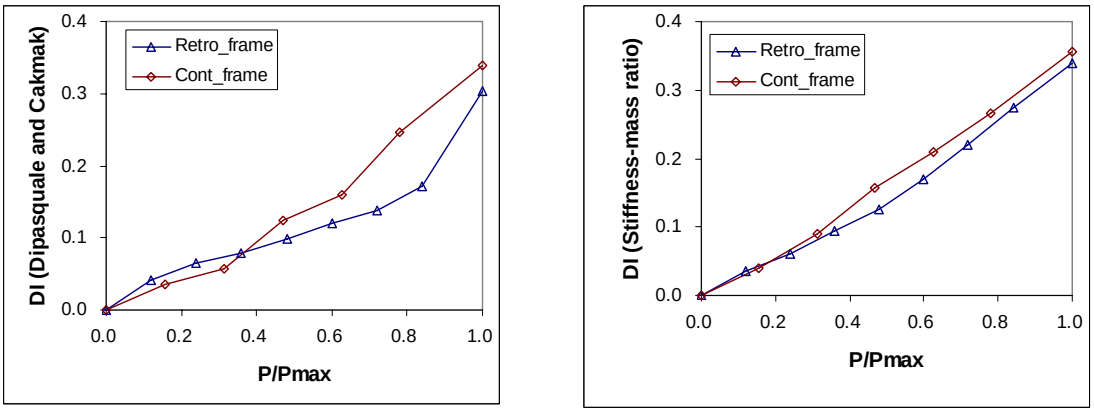

(a) (b)

Figure 16. a) *DI* of Dipasquale and Cakmak plots and b) *DI* of Stiffness-mass ratio plots.

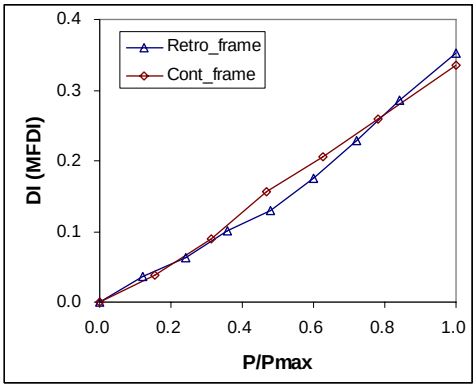

Figure 17. *DI* of Modal flexibility damage method plots.

5.2.2 Retrofitted frame

From Figure 14 and 15, at initial state the natural frequency at first, second and third mode were 6.7Hz, 20.7Hz and 34.0Hz, respectively. At yield point, the frequencies at first, second and third mode were 6.1Hz, 19.3Hz and 32Hz respectively. The yield damage state of the strengthened frame was visible at a load 18kN, DI_{Dip} of 0.14, DI_{SMR} of 0.22 and DI_{MFDI} of 0.23, severe damage state. At ultimate damage state, the frequencies at first, second and third mode were 5.5Hz, 17.2Hz and 29Hz respectively. The damage index of DI_{Dip} was 0.30, DI_{SMR} was 0.34 and DI_{MFDI} was 0.35. The average changed of corresponding resonance frequency decreased approximately 16.51%. The time history plots of retrofitted frame indicate that the stiffness of the damaged control frame is regained significantly by wrapping FRP jacket but it is not able to bridge the cracks fully.

The relation between load and the damage indexes of retrofitted frame are shown in Figure 16 and 17 along with the control frame and details are presented in Table 4. It is clearly shown that the value of DI_{SMR} and DI_{MFDI} are larger than DI_{Dip}. Meanwhile, the index of stiffness-mass ratio and modal flexibility damage method are more accurate and more reliable to estimate structural damage than the modal plastic softening damage index. These

resuls prove that, damage indexes based on modal parameters of retrofitted frame below the curves of control frame indicating better performance. Moreover, both damage indexes based on deformation and change in stiffness show a much acceptable accuracy correlation with modal parameters damage indexes in general. Although damage index based on change in modal parameters work when damage reaches severe stage but this method with the help of impact hammer test is a useful technique to monitor health of structure without destructing when damage is hidden within the structure behind strengthening material layers.

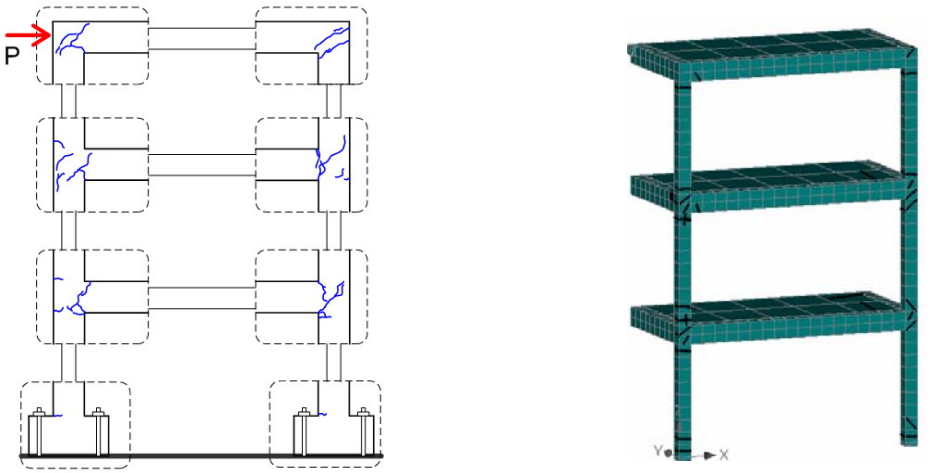

(a) (b)

Figure 18. Failure mode at final state of control frame: a) experimental test and b) FE model

5.3 Failure mechanism

5.3.1 Control frame

Experimental failure modes at final state of control frame at each floor are shown in Figure 18. At yield load, first diagonal cracks started at connection joints of top floor. These opening cracks increased when load was increasing. The second and third diagonal cracks occurred at beam-column connections of second and first floor respectively. It indicated that first plastic hinges were started at top floor and the other hinges were formed at second and first floor respectively. The structure suddenly lost their load carrying capacity when cracks crossed from tension surface though compression surface of structural cross section elements. At final state, both diagonal and flexural cracks were occurred on structural elements of each floor, indicating that the failure mode of control frame was combined between shear mode and flexural mode. Only flexural failure mode was observed at column near stub foundation. The lateral load carrying capacity of control frame was insufficient due to non-ductile reinforcement detailing, which included no beam-column joints transverse reinforcement. Therefore, the top and bottom bars moved in the opposite direction under combined forces. These forces were balanced by bond stress developed between concrete and steel bars. In such circumstances, the plastic hinges were formed by debonded bars and connection joints lost their capacity to carry load.

5.3.2 Retrofitted frame

Debonding of FRP sheets were a failure mechanism for the retrofitted frame. After the yield load, the boned of flexural FRP layers delaminated along the interface between the concrete and FRP sheet. The delamination always started at the corner of beam-column connection in tension zone. The first cracks with their moving sound were initiated at connection of top floor and other cracks were formed at second floor and first floor respectively. After initial debonded FRP sheet formed, the retrofitted structure was stating to lose their load carrying capacity. The FRP sheets of confinement layer suddenly delaminated at ultimate load with their breaking sound. Small cracks were occurred on FRP layers at final state and huge cracks occurred inside existing RC elements behind strengthening layers. The typical failure of retrofitted frame is shown in Figure 19. Again, the primary failure mechanism was debonding of the FRP sheets. It occurred at the base of the huge cracks in tension zone of the damaged RC elements.

(a) (b)

Figure 19. Failure mode of retrofitted frame: a) experimental test and b) FE model

5.4 Results of FE method and comparative analysis

Developed analytical models were validated by comparing the load-displacement results with experimental data. For accuracy results, the stiffness damage index needs to be scale for each damaged element. The parameters used in this index depend on the cross section of the element and in order to use the original parameters for elements with different properties as compared to the experimental elements. This index is modified on the basis of the degradation of elastic modulus and applied to FE model [19]. Figure 20 shows the backbone load-displacement plots from the FE analysis agree well with the experimental results. The model plots were stiffer than that from experimental results. The yield load for the FE analysis of control frame was 13 kN, which was higher than the load of 12.5kN from the experimental results by 4%. Lastly, the ultimate load of 16 kN from model was lower than the ultimate load of 16.5 kN from the experimental data by 3%. Similar to the control frame, the yield load for the model of strengthened frame was 20 kN, which was higher than the actual frame of 18 kN by 11.11%. The ultimate load for the model was 26kN, which was

higher than the ultimate load of 25 kN for the actual frame by 4%. The crack patterns at final state from FE models corresponded well with the observed failure mode of experimental control frame and retrofitted frame after removed FRP sheets.

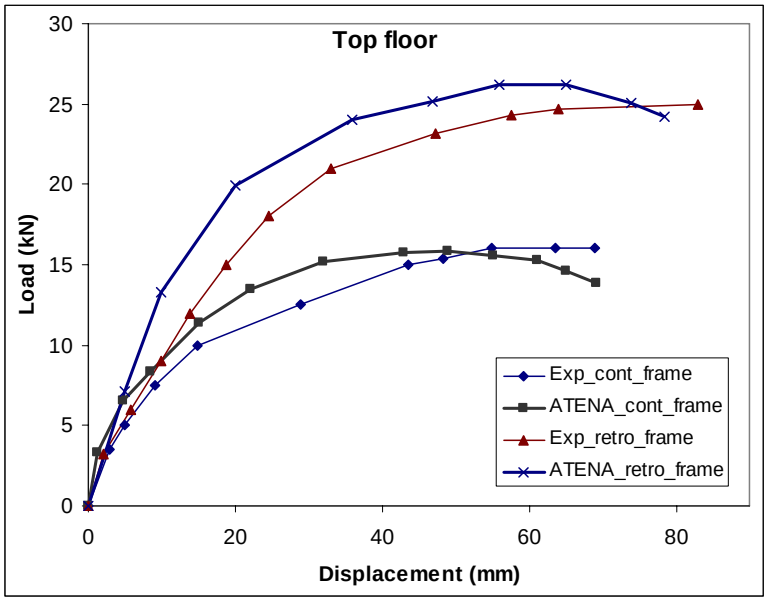

Figure 20. Back bone load-displacement plot between experimental results and FE models.

6. CONCLUSION

Based on the performed research investigation, the following main conclusions can be drawn:

1) Experimental results approve that the use of FRP wrapped for structural strengthening provides increased significant lateral load capacity. The ductile behaviour of the strengthened frame is largely restored after the FRP composite sheets are engaged.

2) The health of RC structures of both original and strengthened specimen seemed to become unsafe when DI_{Park} and DI_k increases larger than 0.5 or dynamical damage indexes increase larger than 0.2. In other hand, the damaged structures are unsafe when structural stiffness reduces to more than 50% of initial state.

3) The damage indexes of strengthened frame reduce indicating better performance as compare to the control frame. Damage indexes based on deformation and change in stiffness show a much acceptable accuracy correlation with dynamical damage indexes in general.

4) Although the stiffness of the damaged RC structure is regained significantly by wrapping FRP jacket but it is not able to bridge the cracks fully. The failure of the strengthened specimen is due to breaking up of the bond between FRP layer and concrete.

5) The analytical results and crack patterns from FE method agree well with the experimental results.

REFERENCES

1. Kanwar V, Kwatra N, Aggarwal P, Gambir ML. Vibration monitoring of a RCC building model, *Proceedings of National Conference on Technology for Disaster Mitigation*, Hamirpur, India, 2006, pp. 277-285.
2. Li A, Assih J, Delmas Y. Shear strengthening of RC beams with externally bonded CFRP sheets, *Structural Engineering*, No. 4, **127**(2001) 374-80.
3. Ghobarah A, Elmandoohgalal K. Seismic rehabilitation of short rectangular RC columns, *Earthquake Engineering*, No. 1, **8**(2004) 45-68.
4. Memon MS, Sheikh SA. Seismic resistance of square concrete columns retrofitted with glass-fiber reinforced polymer, *ACI Structural Journal*, No. 5, **102**(2005) 774-83.
5. Mukherjee A, Joshi M. FRPC reinforced concrete beam-column joints under cyclic excitation, *Composite Structures*, **70**(2005) 185-99.
6. Park YJ, Ang A H-S. Seismic damage analysis of RC buildings, *Structural Engineering ASCE*, Vol. ST4, **111**(1985) 740-57.
7. Powell GH, Allahabadi R. Seismic damage prediction by deterministic methods: Concept and Procedure, *Earthquake Engineering and Structural Dynamic*, **16**(1987) 719-34.
8. Kanwar V, Kwatra N, Aggarwal P. Damage detection for framed RCC buildings using ANN modelling, *Damage Mechanics*, No. 4, **16**(2007) 457-72.
9. Samali B, Li J, Crews KI, Al-dawod M. Load Rating of impaired bridges using a dynamic method, *Electronic Journal of Structural Engineering*, special issue: loading on structure, 2007, pp. 66-75.
10. Dipasquale E, Cakmak AS. Seismic damage assessment using linear models. *Soil Dynamics and Earthquake Engineering*, No. 9, **4**(1990) 194-215.
11. Rodriguez R, Barroso LR. Stiffness-mass ratios method for baseline determination and damage assessment of a benchmark structure, *Proceedings of the American control conference anchorage*, AK, USA, 2002, pp. 2469-2474.
12. Wang JF, Lin CC, Yen SM. Story damage index of seismically-excited buildings based on modal parameters, *18th International Conference on Structural Mechanics in Reactor Technology*, Beijing, China, 2005, pp. 3278-3289.
13. Ko JM, Sun ZG, Ni YQ. Multi-stage identification scheme for detecting damage in cable stayed Kap Shui Mun bridge, *Engineering Structures*, **24**(2002) 857-68.
14. Estekanchi H, Arjomandi K. Comparison of damage indexes in nonlinear time history analysis of steel moment frames, *Asian Journal of Civil Engineering*, No. 6, **8**(2007) 629-46.
15. Pandey AK, Biswas M. Damage detection in structure using changes in flexibility, *Sound and Vibration*, No. 1, **169**(1994) 3-17.
16. Perez JJ, Zhao L, O'Riordan-Adjah CA. Finite element evaluation of the effects of lateral anchorage strips on the behaviour of CFRP-strengthened RC beams, *Proceedings of the international symposium on bond behaviour of FRP in structures*, Chen and Teng, International institute for FRP in construction, 2005, pp. 303-308.
17. Supaviriyakit T, Pornpongsaroj P, Pinmanmas A. Finite element analysis of FRP-strengthened RC beams, *Songklanakarin Journal of science and technology*, No. 4,

26(2004) 497-507.
18. Kachlakev D, Miller T, Yim S. Finite element modeling of reinforced concrete structures strengthened with FRP laminates. *Final report-SPR 316*, Oregon department of transportation and Federal highway administration, 2001.
19. Lee U, Shin J. A frequency response function-based structural damage identification method, *Computers and Structures*, **80**(2002) 117-32.